Glacier thickness modelling and monitoring with geophysical data constraints: A case study on the Indren Glacier (NW Italy)

Received: 3 September 2024 | Revised: 20 December 2024 | Accepted: 24 December 2024

DOI: 10.1002/esp.6068

CASE STUDY

ESPL WILEY

Glacier thickness modelling and monitoring with geophysical data constraints: A case study on the Indren Glacier (NW Italy)

Valeria Strallo[1] | Chiara Colombero[1] | Fabrizio Troilo[2] | Luca Mondardini[2] | Alberto Godio[1]

[1]Department of Environmental, Land and Infrastructure Engineering (DIATI), Politecnico di Torino, Torino, TO, Italy

[2]Fondazione Montagna Sicura, Courmayeur, AO, Italy

Correspondence
Strallo Valeria, Politecnico di Torino, Department of Environmental, Land and Infrastructure Engineering (DIATI), Torino (TO), 10129, Italy.
Email: valeria.strallo@polito.it

Funding information
MUR, Grant/Award Number: DM 118/2023

Abstract

The ongoing global temperature increase has accelerated the mass loss of glaciers worldwide, with Italian alpine glaciers being particularly vulnerable due to their small size, complex geometries and exposition that implies a fast reaction to thermal and hydrological modifications. In such a frame, the Indren Glacier (Aosta Valley, north-western Italian Alps) provides a valid test site to check the thickness evolution over the last two decades (1999–2020), through an integrated approach combining historical data, on-site geophysical measurements, remote sensing surveys, modelling and temperature analysis. Using a 2018 helicopter-based photogrammetric survey and Ground Penetrating Radar (GPR) survey campaigns of 2020, we obtained new input data and constraints to build up an updated thickness model for the whole glacier through the Glacier Thickness Estimation algorithm (GlaTE). Ice thickness is indeed a key parameter to estimate the ice volume and use it as further input in evolutionary models forecasting future scenarios. As a part of this integrated approach, we also analysed remote sensing and temperature data, finding a major modification in the glacier conditions over the last decade. Further comparing these results with previous studies, we identified a significant decrease in ice thickness, and we confirmed the presence of an over-deepening in the glacier central widest part. This integrated methodology enhances our understanding of glacier dynamics and improves predictions of future changes, offering crucial insights for managing water resources and mitigating natural hazards in the alpine region.

KEYWORDS
Alpine glaciers, Climate change, Glacier Thickness Estimation algorithm (GlaTE), Ground-penetrating radar (GPR), Ice thickness estimation, Indren Glacier

1 | INTRODUCTION

The continuous increase in global mean temperatures and the decrease in snow precipitation at high altitudes over the last years have caused the mass loss of ice bodies all over the world (IPCC, 2019; Lemke et al., 2007). Mountain or alpine glaciers show a higher reactivity to climate compared to glaciers at lower elevations (Owen et al., 2009; Pepin et al., 2015; Solomon et al., 2007). Their high vulnerability to both present climatic conditions and future scenarios is primarily associated with their small size, steepness, dynamic behaviour and relatively high temperatures, typically just a few degrees Celsius below zero (Colombero et al., 2019; Harris et al., 2009; Huss & Fischer, 2016; Winkler et al., 2010; Zemp & Haeberli, 2007). European Alps, in particular, have already lost almost 50% of their total glacial area from 2000 and will continue experiencing severe shrinkage by the end of the 21st century (Hanzer et al., 2018; Zemp et al., 2006).

Melting of mountain glaciers can cause serious natural hazards linked to slope stability, like glacier floods, rock slides, as well as the outburst of glacial lakes, threatening nearby communities and

infrastructures (Harris et al., 2009; Hock et al., 2019; Kääb, Reynolds, & Haeberli, 2005). Concerning Alpine glaciers, which are a key source for the European hydrological regime, the effects of their shrinkage impose severe environmental and socio-economic impacts both at local and global scales (Gobiet et al., 2014; Linsbauer, Paul, & Haeberli, 2012; Salim et al., 2021; Zekollari, Huss, & Farinotti, 2019; Zemp & Haeberli, 2007). Previous studies have shown how the continuous ice melting of these bodies, will place pressure on water resources (Beniston & Stoffel, 2014). This will cause a shift in the hydrological regime and a decrease in the mean annual river runoff, strongly affecting water supply, agriculture, hydropower generation and ecosystem equilibrium (Beniston et al., 2018; Brown, Hannah, & Milner, 2007; Horton et al., 2006; Milner et al., 2017; Patro, De Michele, & Avanzi, 2018; Zemp & Haeberli, 2007).

Given alpine glacier's role as reliable climatic indicators, focusing research efforts on these vulnerable environments is essential to understand the cryosphere-climate interactions and for modelling future scenarios (Haeberli, 2005; Haeberli et al., 2017; Mark & Fernández, 2017). Studies conducted in the alpine region could also provide a foundation for understanding the evolution of other remote glacial bodies, especially in cases where survey campaigns and data acquisition would be more challenging.

The ice thickness of a glacier represents a key parameter for its characterization and the estimation of ice volume. This latter is the starting point for assessing the glacier's dynamics and forecasting its future evolution in response to climate forcings (Gärtner-Roer et al., 2014; Rabatel et al., 2018). While the thickness decrease and the overall shrinkage can be monitored from remote sensing surveys, accurately quantifying the ice thickness at a specific time frame still presents significant challenges. Geophysical investigations, and in particular Ground Penetrating Radar (GPR) surveys, have demonstrated to be a powerful tool for this purpose, leading to accurate areal results in a fast and cost-effective way (Binder et al., 2009; Singh et al., 2012). In temperate glaciers, scattering phenomena of the electromagnetic (EM) signal can occur in water-rich regions or volumes of warm ice. These regions have dielectric permittivity that differs significantly from that of pure ice, causing the signal to deviate in multiple directions and creating High Scattering Zones (HSZ) and energy loss (Colombero et al., 2019; Forte et al., 2021; Ogier et al., 2023; Santin et al., 2024). Further logistical constraints and site accessibility in the presence of severe crevassing often prevent exhaustive on-site surveys. As a result, the obtained data might be sparse or confined to limited areas of the glacier, thus failing to fully outline the glacier's bottom morphology and leading to the need of modelling tools to laterally extend the estimation.

Different methodologies for the modelling of glacier's thickness are found in the literature; among all the possible modelling approaches, we focus on the Glacier Thickness Estimation algorithm (GlaTE), developed by Langhammer et al. (2019), because of its high flexibility and low demand for input data. In addition, the theoretical model of thickness can be constrained with experimental data, particularly GPR surveys, to obtain accurate estimates. Other models can be applied to forecast the temporal evolution of ice thickness, implying calibration and validation over historical data and more complex input requirements (Van Tricht & Huybrechts, 2023; Zekollari et al., 2022; Zekollari, Huss, & Farinotti, 2019). From the monitoring perspective, the combination of remote sensing data (e.g., Digital Elevation Models) and temperature trend estimations may provide important insights to estimate thickness variability over time. This approach is advantageous because it is faster and requires fewer constraints compared to complex modelling.

An integrated approach involving on-site geophysical measurements, remote sensing acquisitions, modelling and meteorological data analysis is well-established in glaciological studies, providing a robust framework for analysing ice thickness evolution in response to climate modifications. In this study, we demonstrate the effectiveness of this approach by applying it to the Indren Glacier (Aosta Valley, northwestern Italian Alps) to evaluate its changes over the last two decades (1999–2020).

2 | MATERIALS AND METHODS

For the estimation of the Indren Glacier's ice thickness and its evolution, we employed a comprehensive methodology, integrating remote sensing data, geophysical instruments and modelling techniques.

We began by collecting freely accessible historical data, previous on-site measuring campaigns and modelling attempts. Specifically, Viani et al. (2020) already applied the Glacier Bed Topography Model (GlabTop, Linsbauer, Paul, & Haeberli, 2012) to estimate the ice thickness of the same glacier. This was achieved using the regional Digital Terrain Model (DTM) from 1991 and the glacier perimeter from the same year as model inputs. This study identified a potential overdeepening in the central part of the glacier. Similar results are available from the Regional Agency of Environmental Protection of the Aosta Valley Region (https://mappe.partout.it/pub/GeoNavSCT/?repertorio=arpa, last accessed on September 3, 2024), obtained using the same unconstrained modelling tool (GlabTop) and remote sensing inputs (DTM and perimeter) from 2008 for all the glaciers across the region. To use more recent input data for the modelling, we used the updated glacier perimeter and high-resolution DEM obtained from a helicopter-based photogrammetric survey of the glacier carried out in 2018. We then conducted a denser GPR campaign on the Indren Glacier in July 2020, with the aim of validating the previous results and introducing experimental constraints into the modelling of ice thickness. Despite the challenges in interpreting the GPR data in some portions of the glacier, we used the new geophysical data as a constraints in the GlaTE algorithm of Langhammer et al. (2019) and compared it with previous studies. Additionally, we linked the analysis of the available DTMs and DEM over the years with a detailed analysis of air temperature measured at the nearest meteorological monitoring stations, to quantify the thickness evolution over the same time period.

2.1 | Test site: the Indren glacier

The Indren Glacier is located at the top of the Lys and Sesia valleys, in the Aosta Valley region, at the border with Piedmont (Figure 1a). It is found on the Monte Rosa massif, which belongs to the Italian Pennine Alps. The glacier is south-west oriented and located at the foot of the Vincent Pyramid, with elevations ranging from 3,000 m to 4,200 m approximately (Figure 1b; Colombo et al., 2019; Freppaz et al., 2021; Maggioni et al., 2009; Tognetto et al., 2021). In the frontal portion, it feeds the Lys stream and is in direct contact with a proglacial pond

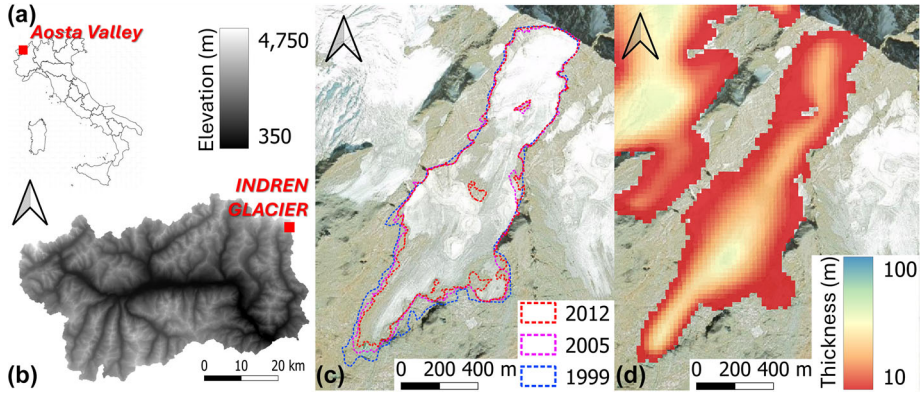

FIGURE 1 (a) Geographical location of the Indren Glacier (Aosta Valley, northwestern Italian Alps). (b) DTM of the Aosta Valley region from 1999 (https://mappe.regione.vda.it/pub/geonavitg/geodownload.asp?carta=DTM99, last access on September 3, 2024). (c) Glacier perimeters available on the historical regional database (http://catastoghiacciai.partout.it/, last access on September 3, 2024). (d) Glacier thickness estimation through GlabTop model using the regional DTM of 2005–2008 and the glacier perimeter of 2005 as inputs.

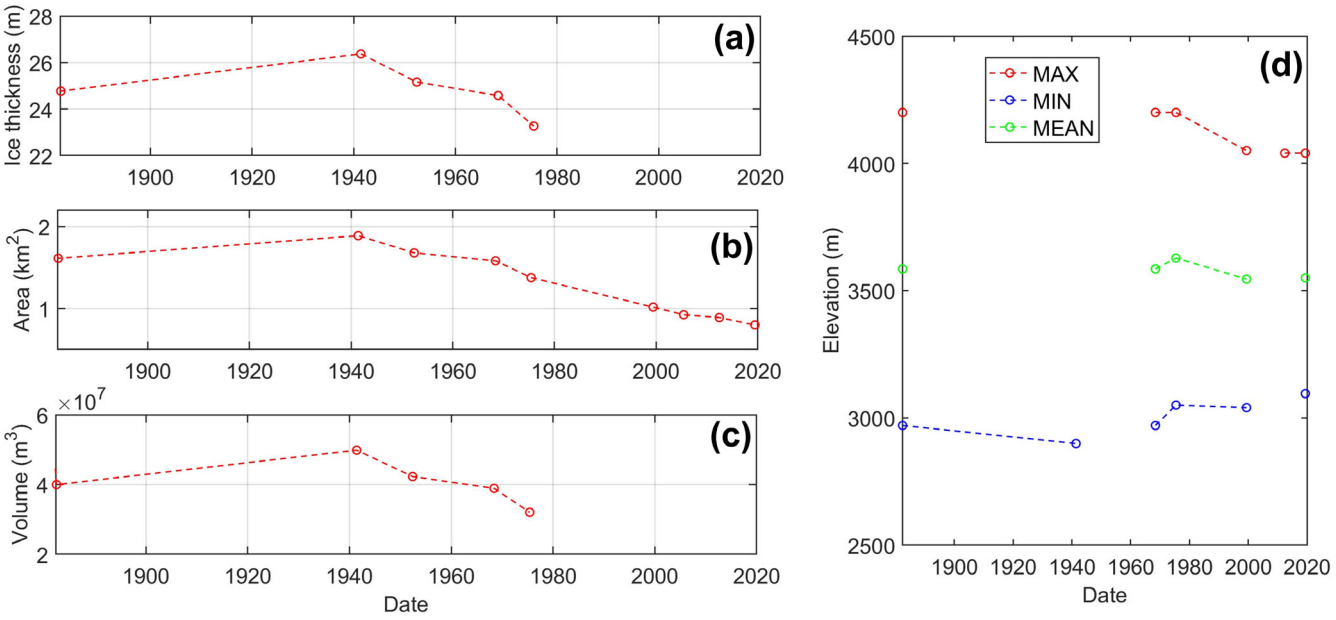

FIGURE 2 Discontinuous historical data (1882–2020) on (a) average ice thickness; (b) area; (c) estimated volume; (d) minimum, maximum and average elevation of the Indren glacier, available on the historical regional database (http://catastoghiacciai.partout.it/, last access on September 3, 2024).

having an extension of approximately 1 km^2. Starting from 1850, the glacier front has retired of 1 km with a retreat of approximately 500 m between 1927 and 2013 (Colombo et al., 2019; Godio et al., 2017). The available historical perimeters of the glaciers over the first decade of analysis (1999–2012) are shown in Figure 1c (http://catastoghiacciai.partout.it/, last access on September 3, 2024). Notably, signification variations in the glacier area have occurred along the years and the ice thinning in the upper central area led to the exposure of a few rock outcrops.

Figure 1d displays the ice thickness of the glacier modelled with GlabTop (Linsbauer, Paul, & Haeberli, 2012) obtained for all the glaciers of the region with input data from 2005 to 2008 and without experimental data constraints. The possible over-deepening is visible in the axial lower portion of the glacier.

Historical data on the average ice thickness, area and volume decrease over years are available for the Indren Glacier in the same regional database (http://catastoghiacciai.partout.it/, last access on September 3, 2024). All the available data are summarized in Figure 2, together with the historical variations in minimum, maximum and average elevation. As expected, a clear decreasing trend is found for the ice thickness, area and volume starting from the measurements of 1940. As a consequence, the minimum elevation of the glacier has slightly increased over the years. Apart from the GlapTop models mentioned above (referred to 1991 and 2008 input data), there is no additional information on ice thickness related to recent years. This leak of data led us to develop a methodology to obtain an updated ice thickness model for the site.

2.2 | DEM reconstruction and analyses

We used the available regional DTMs covering the glacier area to track potential variations in the glacier thickness over the period 1999–2018.

The available regional DTM-1999 was obtained through the interpolation of elevation data and contour lines present in a large-scale technical map of the Aosta Valley (orthometric heights, reference system UTM ED50 zone 32 N). The final resolution of this dataset is 10 m.

The second DTM of the region, referred to as DTM-2008, was created by merging two separate datasets collected during different periods. The first dataset, acquired in 2005–2006, focused on areas susceptible to debris flow hazards and the main fluvial areas within the region. This dataset offers a high resolution of 0.5 m (orthometric heights, reference system UTM ED50 zone 32 N). The second dataset, acquired in 2008, completed the coverage of the remaining parts of the region that were not scanned in the initial survey, including the area of the Indren Glacier. This dataset has a resolution of 2 m (orthometric heights, reference system UTM ED50 zone 32 N). Both datasets were acquired using a LiDAR (Light Detection and Ranging) scanner mounted on board of an aerial platform.

A high-resolution DEM of the Indren glacier was finally obtained in July 2018 by Fondazione Montagna Sicura (FMS), through an aerial photogrammetric flight (DEM-2018).

The DEM-2018, covering the whole glacier surface, was obtained by performing a helicopter flight and acquiring oblique digital images with a Sony DSC-HX90 digital camera. The surveyed area covered 3.54 km^2, obtaining an orthomosaic with a ground resolution of 18.5 cm/pixel and a DEM with a ground resolution of 36 cm/pixel. The image processing was performed by applying Structure from Motion Algorithms with the use of Agisoft Metashape software. A total of 19,879 tie points were identified using 25 images, which were then used to generate a dense cloud of 9,199,227 points. From the dense cloud, we derived the DEM and the orthomosaic products. Four Ground Control Points were used. Three of these points were used to produce the external orientation of the photogrammetric model. The fourth point, centrally positioned, served as a checkpoint to assess the error of the model. The error was found to be equal to 0.81 m on the XY plane and 0.36 m on the Z axis.

This dataset has a final resolution of 0.4 m (ellipsoidal heights, reference system WGS84 UTM zone 32 N). We used this DEM, together with the glacier perimeter manually defined on the orthomosaic of the same survey (Figure 4), to model the updated ice thickness constrained with GPR data of 2020.

Figure 3 shows the three models, cut over the perimeters of the glacier in the different reference years.

To highlight thickness variations over the two decades, comparisons were made between the available elevation models (2008–1999, 2018–2008 and 2018–1999). All layers were converted to the WGS84 UTM zone 32 N reference system, and DEM-2018 elevations were converted to orthometric heights to allow for comparison with the regional data. To overcome limitations due to differences in resolution between the three surveys, a smoothing procedure was applied. In particular, the layer differences involving the DTM-1999 (10-m resolution) were low-passed filtered to contrast artefacts related to the grid dimensions.

2.3 | GPR data set

The ground-based GPR dataset was acquired in two different survey campaigns of July 2020 (Figure 4). The first dataset consisted of 12 profiles acquired over the area of potential thickness over-deepening and the frontal part of the glacier (Figure 1d). A 200-MHz IDS antenna connected to an IDS K2 TR200 acquisition unit was used in this campaign. The antenna was manually dragged on the snow surface and GPR traces were georeferenced by means of a GNSS RTK antenna (Emlid Reach RS2+) mounted on the radar antenna. GPR traces were recorded for a total length of 800 ns, with a sampling of 2048 samples/trace. The second survey campaign was carried out with the same system and acquisition parameters, but mounting a 70-MHz antenna (Subecho-70, Radarteam). This selection was done in order to achieve a potentially higher investigation depth in the area of the over-deepening and upwards, where scattering and attenuation

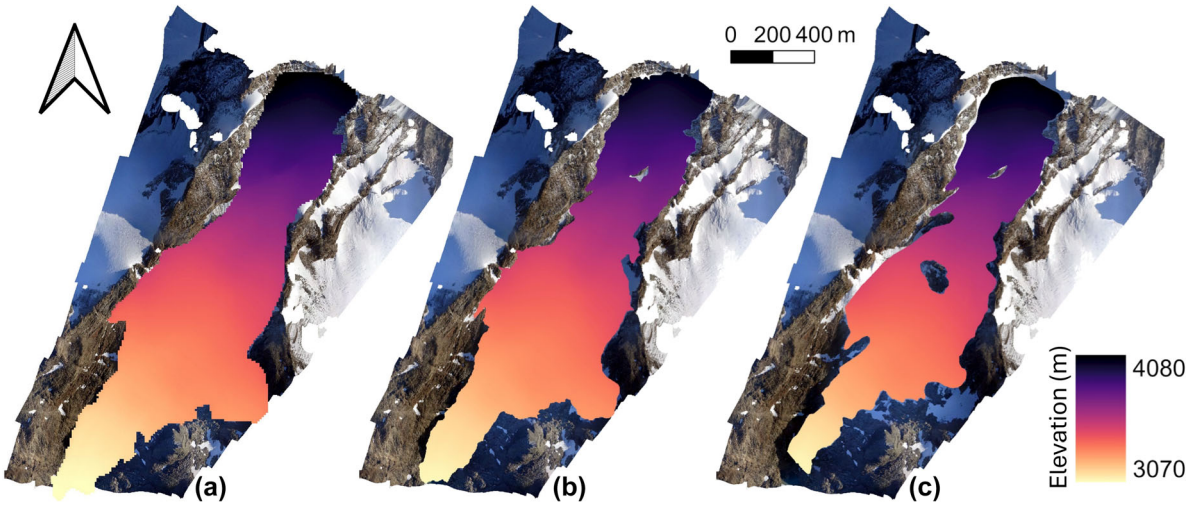

FIGURE 3 Regional DTMs (1999 (a) and 2008 (b)) and local DEM (2018 (c)) cut on the glacier perimeters of the different years, overlapped to the glacier orthophoto retrieved from the photogrammetric flight of 2018. DTM-1999 and DTM-2008 are available from https://mappe.regione.vda.it/pub/geonavitg/geodownload.asp?carta=DTM99, last access on September 3, 2024. Glacier perimeters for years 1999 and 2008 are available on the historical regional database (http://catastoghiacciai.partout.it/, last access on September 3, 2024). The perimeter of 2018 was manually picked on the orthomosaic of the photogrammetric flight.

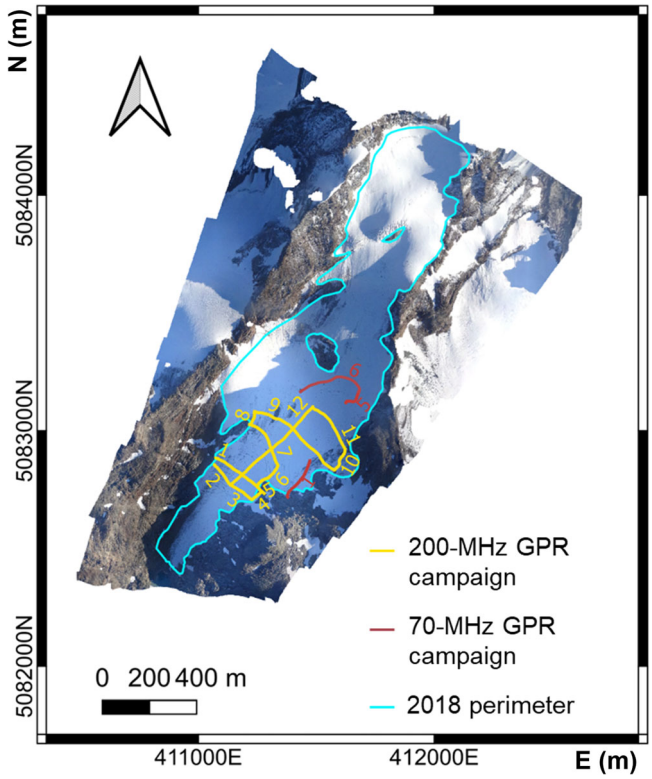

FIGURE 4 Orthophoto and glacier perimeter obtained from photogrammetry (2018) with the location of the GPR profiles acquired in July 2020 for which thickness information could be retrieved even in partial segments of the profiles.

partially compromised the interpretation of the profiles acquired during the first campaign. However, the quality of this second dataset was very poor and only three of the seven available profiles (lines 1, 5 and 6 in Figure 4) led to additional information about the glacier bottom morphology and ice thickness.

We considered a constant velocity of 0.17 m/ns (EM wave propagation velocity in ice) for time-to-depth conversion, disregarding the presence of a shallow thin and discontinuous snow cover. With this velocity, the wavelengths of the two survey campaigns are approximately 0.85 m and 2.43 m, implying indicative vertical resolutions (wavelength/4) of 0.2 m and 0.6 m (Annan, 2003).

A standard processing procedure was applied to the raw radargrams. The start time of each trace was shifted to delete samples preceding the initial pulse and obtain the exact zero time. A high-pass filter was applied to remove the low-frequency noise (dewow). The average trace of each radargram was subtracted to remove the horizontally coherent noise. Traces were further corrected for geometrical spreading, to gain signal amplitude with depth. We manually removed the stationary traces inside the radargrams caused by random stops in the dragging of the antenna close to crevasses and in other difficult walking conditions and applied time-to-depth conversion. Finally, we proceeded with the migration of the GPR data to improve the bottom visualization and remove the presence of diffraction hyperbola. For this purpose, we applied a Kirchhoff migration with a summation width of 200 traces.

A manual picking of the ice bottom reflections was performed on the processed radargrams, to map the glacier thickness along the profiles.

2.4 | Ice thickness modelling with GPR data constraints

Given the availability of an updated glacier geometry (perimeter and elevations) and thickness measurements obtained from the GPR data, we selected the GlaTE algorithm (Langhammer et al., 2019) as the optimal modelling tool for extending the thickness estimation to the entire glacier area. Through an inversion procedure, this model aims at reducing the mismatch between the ice thickness estimated by means of a starting theoretical model and the experimental measurements acquired through GPR. The GlaTE model can incorporate any glaciological model from the literature as its theoretical constraints. Here, we considered the approach developed by Clarke et al. (2013), i.e., the same used by the authors of the GlaTE algorithm. The initial glaciological model links the basal shear stress (τ) to the ice thickness and geometry of the glacier. However, the parameters defining τ might be highly variable, a correction factor based on the minimization of the difference between measured (through GPR) and estimated thickness is therefore introduced. The model is further constrained at the glacier perimeter (i.e., thickness = 0 m) and a regularization constraint is introduced. This strategy aligns with Occam's principle, favouring simpler solutions amidst the model's multiple outputs. By applying relative weights to the different constraints, the model allows to allocate the confidence in all the individual contributions.

We used the glacier perimeter and DEM related to 2018 as model inputs. The DEM was resampled to a coarser, but homogeneous, cell size of 5 m to speed up the computational processing and avoid local artefacts. The thickness data retrieved from the GPR survey campaigns of 2020 were then used as model constraints.

2.5 | Temperature analysis

To complete the analysis of the long-term evolution of the glacier thickness, we used the freely available air temperature measurements of the closest meteorological stations to estimate a temperature trend for the period 1999–2020 (Table 1). The station BP (Bocchetta delle Pisse) is the one having the longest temperature record, starting in 1988, however, it is located at a significantly lower elevation (−600 m with respect to the glacier front). The station G (Gabiet) is located at a similar elevation at a comparable distance to the glacier, but the temperature record started in 2002. The closest station is CM (Capanna Margherita), having an elevation of +250 m with respect to the glacier summit, but data is limited to the period 2002 to the present. Given the limitations in the available information, we carried out temperature analyses on all the stations to compare the results and obtain an average estimation of the temperature trend over the years.

In detail, we considered daily average temperatures from each station over all the available monitored years. Figure 5 shows the processing procedure aimed at linear fitting the residual temperatures, after the removal of the seasonal components, specifically for the station BP. We filled the gaps in the long-term records (Figure 5a) by replacing the missing daily temperatures with the average temperature for that specific day of the year computed on the whole dataset. We cut the data to complete year periodicity to avoid unbalanced representativeness of some periods of the year (Figure 5b). We then

TABLE 1 Meteorological stations of the regional monitoring networks with available daily average air temperature measurements. The approximate station coordinates are given in WGS84 UTM32N to compute the average distances from the Indren Glacier perimeter. Data sources: ARPA Piemonte for stations BP and CM (https://www.arpa.piemonte.it/rischi_naturali/snippets_arpa_graphs/map_meteoweb/?rete=stazione_meteorologica) and Regione VdA (https://presidi2.regione.vda.it/str_dataview_download) for station GA, last access on September 3, 2024.

Station ID	Station name	Data source	E (m)	N (m)	Elevation (m)	Distance (km)	Data availability
BP	Bocchetta delle Pisse	ARPA Piemonte	414,878	5,080,207	2,410	4.2	1988 to present
CM	Capanna Margherita	ARPA Piemonte	412,940	5,086,616	4,554	2.4	2002 to present
GA	Gabiet	Regione VdA	410,521	5,077,548	2,379	4.8	2002 to present

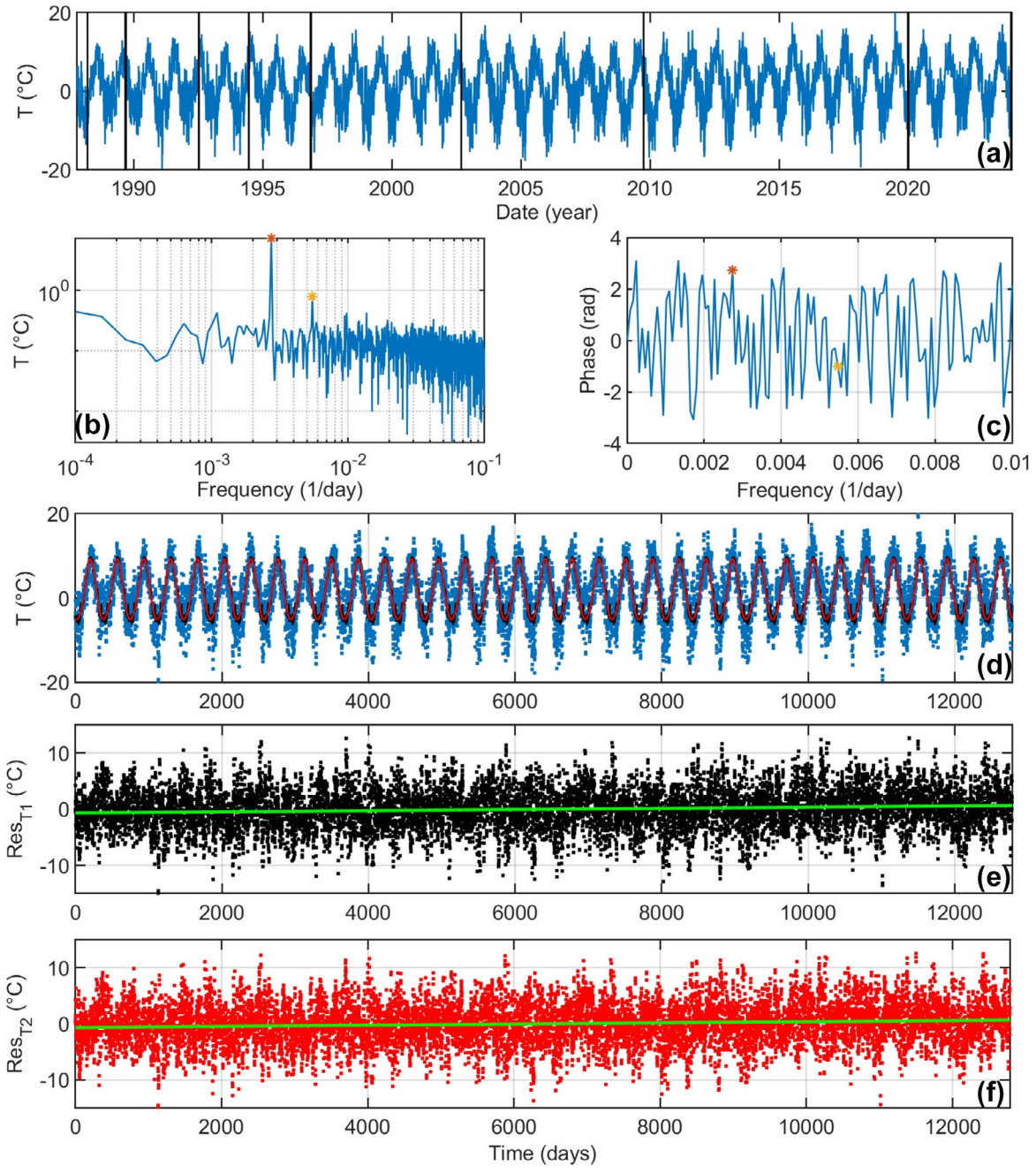

FIGURE 5 Processing of daily average air temperatures recorded at the meteorological stations closest to the Indren Glacier. (a) Raw data for station BP, the black lines highlight periods in which data are not available. (b) Amplitude spectrum and (c) phase spectrum of the data in (a). (d) BP data (cut to complete years) and after gap filling (blue dots) compared to the periodic components retrieved from the daily average temperatures computed over the whole period (in black) and from equation 1 (in red). (e) Residual temperatures after removal of the average temperatures, and related linear fitting line (in green). (f) Residual temperatures after removal of the periodic component retrieved from equation 1, and related linear fitting line (in green).

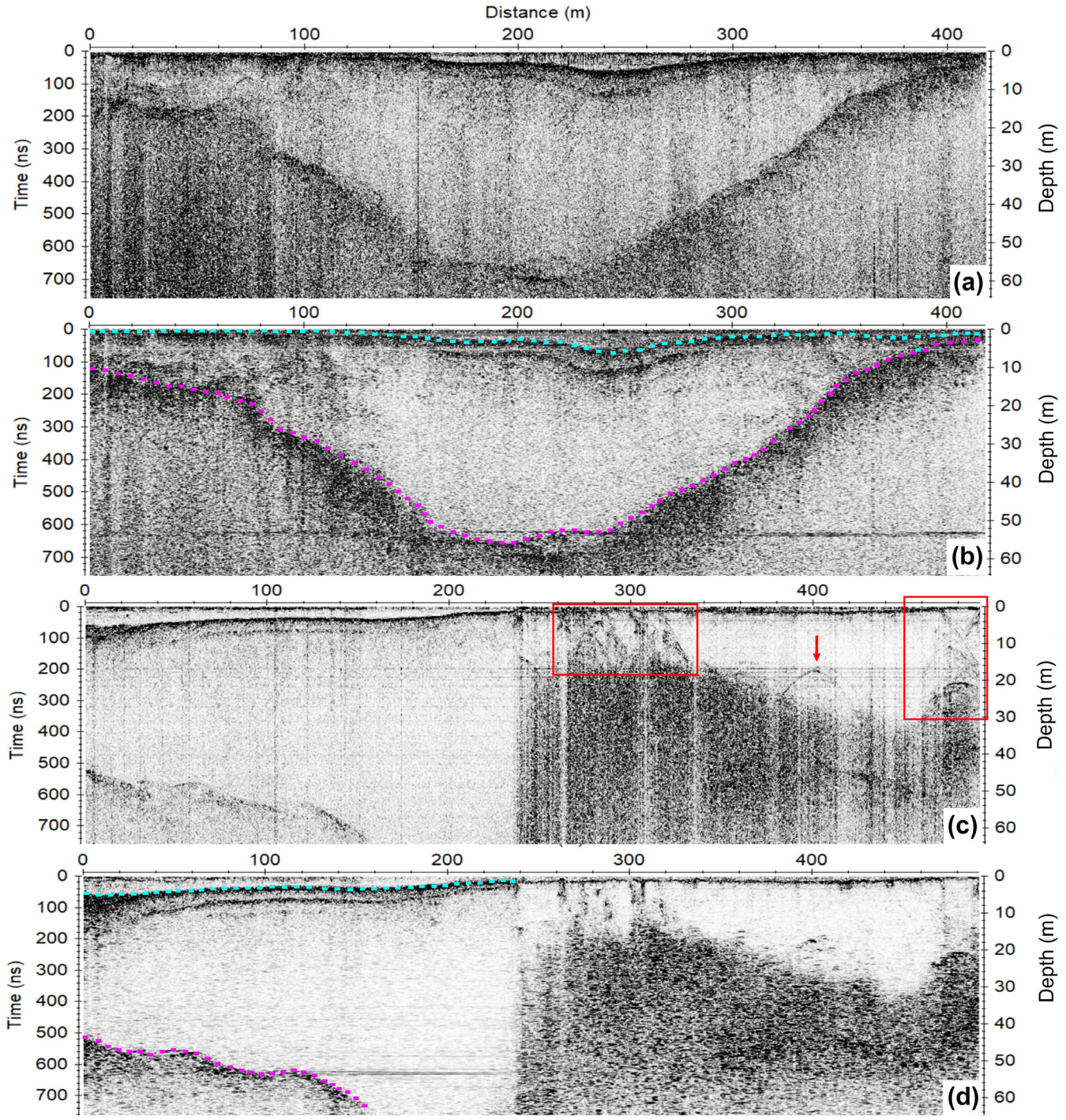

FIGURE 6 GPR results obtained in the 200-MHz survey campaign. (a) Processed radargram of profile 9 (location in Figure 4) prior to migration. (b) Processed radargram of profile 9 with migrated data; interpretation lines of the glacier bottom morphology (in magenta) and snow cover (in cyan). (c) Processed radargram of profile 12 (location in Figure 4) prior to migration; the red boxes indicate widespread diffraction hyperbolas under which intense scattering of the signal is found, and likely related to the presence of crevasses and cavities, whereas the red arrow might indicate the presence of a boulder or a small cavity in the ice matrix. (d) Processed radargram of profile 12 with migrated data; interpretation lines of the glacier bottom morphology (in magenta) and snow cover (in cyan).

estimated the periodical seasonal variations with two different approaches: i) computing the average temperature of each day of the year on the whole dataset, ii) taking advantage of signal processing tools. For the latter, we expressed the periodic component ψ of the data as a sum of cosine functions, the following:

$$\psi = A_1 \cos(2\pi f_1 t + \phi_1) + A_2 \cos(2\pi f_2 t + \phi_2) \quad (1)$$

where t is time (in days), f_1 and f_2 are the two main frequency components detectable in the data, A_1 and A_2 are their related amplitudes, ϕ_1 and ϕ_2 are their related phases. The dominant frequencies with related amplitudes and phases can be easily retrieved from the amplitude and phase spectra of the temperature signal. An example is shown in Figure 5b,c for the station BP (amplitude and phase spectra, respectively). The amplitude spectrum shows a clear dominant peak at a frequency of 0.0027 day^{-1} (f_1), corresponding to a period of

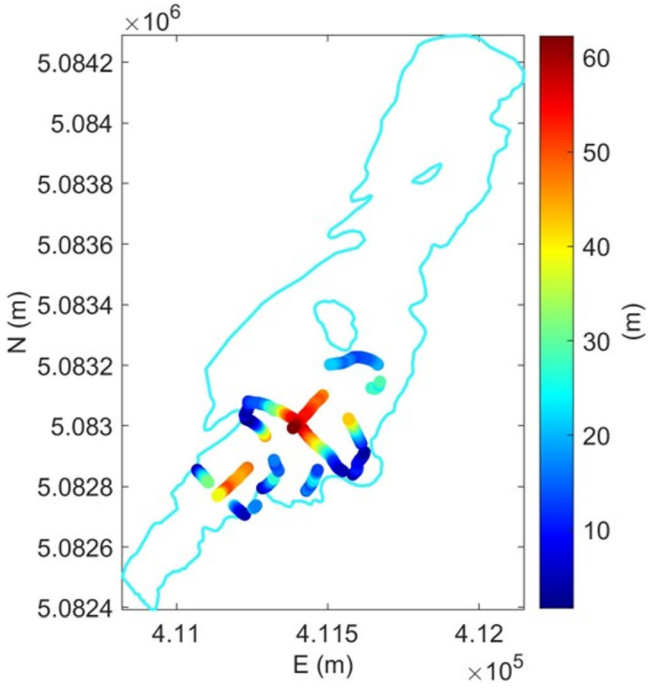

FIGURE 7 Experimental ice thickness retrieved from the GPR investigations along the profiles.

365.25 days. This peak confirms the dominant yearly periodicity in the temperature records. A second peak (f_2) is found at 0.0057 day^{-1}, corresponding to a six-month periodicity. The amplitudes and phases of these two periodic components (f_1 and f_2) can be easily retrieved from Figure 5b,c, respectively, and input in Equation 1.

The periodic components retrieved from the daily average temperature and from signal processing are compared in Figure 5d. The residuals obtained by subtracting each of the period components from the original data are displayed in Figure 5e,f, together with their linear fits. The temperature trend can be easily estimated from the slope of the fitting lines.

We applied this procedure to the three datasets of the closest meteorological stations. Since the station BP provided the longest time record and the methodology was found to be robust with both approaches, we split the long-term records into two subsets to get an approximate reference trend for the two decades under investigation (1999–2008 and 2008–2018). Finally, we performed a direct comparison with the thickness variations highlighted by the DTM and DEM analyses.

3 | RESULTS

This section presents the key findings from our analysis. We begin by presenting the results from the GPR surveys, followed by the integration of the GPR data into the glaciological model. Next, we show the findings from the DTM analysis and conclude with the analysis of the temperature trends.

3.1 | Ice thickness from GPR data

Figure 6 shows representative processed radargrams of two profiles obtained during the survey campaign with the 200-MHz GPR antenna. In particular, Figure 6a,b refers to the longest section transversally cutting the glacier (profile 9 in Figure 4), while Figure 6c,d refers to the longest section acquired along the central axis of the glacier in longitudinal direction (profile 12 in Figure 4). The figure shows processed profiles before and after data migration. Unmigrated data are included because the presence of diffraction hyperbola helps in identifying localized objects, like crevasses, boulders and possible cavities. Data migration generally improved the visualization of the deeper features, but it also enhanced noise artefacts, such as the horizontal stripe at approximately 600 ns in Figure 6b. Further 200-MHz GPR profiles, the longest after lines 9 and 12, are reported in the Supplementary Material (S2–S4).

With the exception of profile 9 (Figure 6a,b), it was not possible to visualize the bottom interface of the glacier along the whole GPR profiles. Intense scattering and attenuation of the GPR signal were encountered in many areas of the processed sections, as clearly shown along profile 12 in Figure 6c,d, from a distance of 240 m.

Despite the diffuse scattering, the thickness measures that could be reconstructed along the profiles are summarized in Figure 7. The ice thickness reaches a maximum depth of approximately 60 m in the central area of the survey, confirming the existence of an overdeepening in this portion of the glacier already identified from glaciological models in the previous studies referred to years 1991 (Viani et al., 2020) and 2008 (Figure 1d).

3.2 | Ice thickness modelling with GPR data constraint

The available GPR thickness constraints were used as inputs to the GlaTE model, together with the updated DEM and perimeter of the glacier retrieved for 2018. Figure 8 displays the modelling results obtained with a smoothing factor of 20 (over E and N distances of 100 m), in compliance with the average spacing between the acquired GPR profiles. The ice thickness estimation from the glaciological model only (h^{glac}) is shown in Figure 8a. Figure 8b displays the interpolation of the GPR data (h^{GPR}) used as constraints, to obtain the final model (h^{est}) of Figure 8c. The difference in thickness between the final model and the unconstrained one is shown in Figure 8d ($h^{est} - h^{glac}$).

3.3 | DTM/DEM analysis

Figure 9 shows the differences in elevation between the available DTMs and DEM of the glacier, over the two considered decades (first decade, 2008–1999, in Figure 9a; second decade, 2018–2008, in Figure 9b; whole period, 2018–1999, in Figure 9c).

3.4 | Temperature analysis

The results of linear fitting on the residual temperatures, obtained after the removal of the seasonal periodic components, are summarized in Table 2. All the fitting lines showed a p-value lower than 10^{-3} for the slope estimates (Figure 5e,f), meaning negligible probability of having zero-slope fitting curves. The trend in the data should therefore be

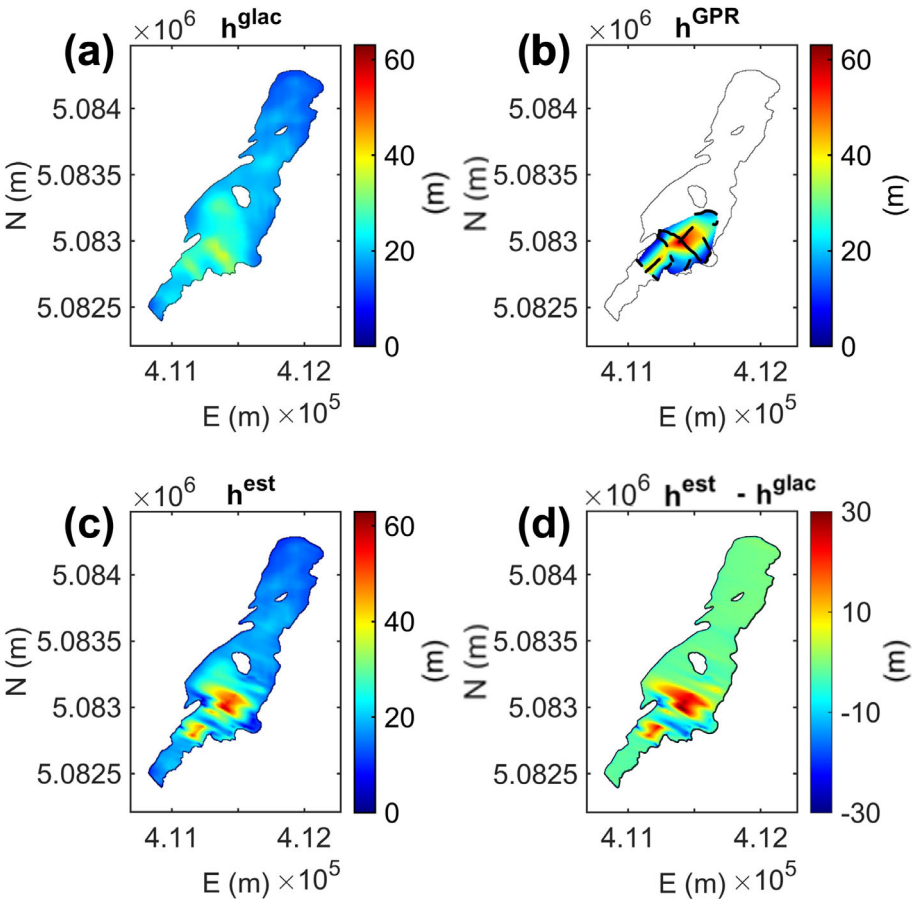

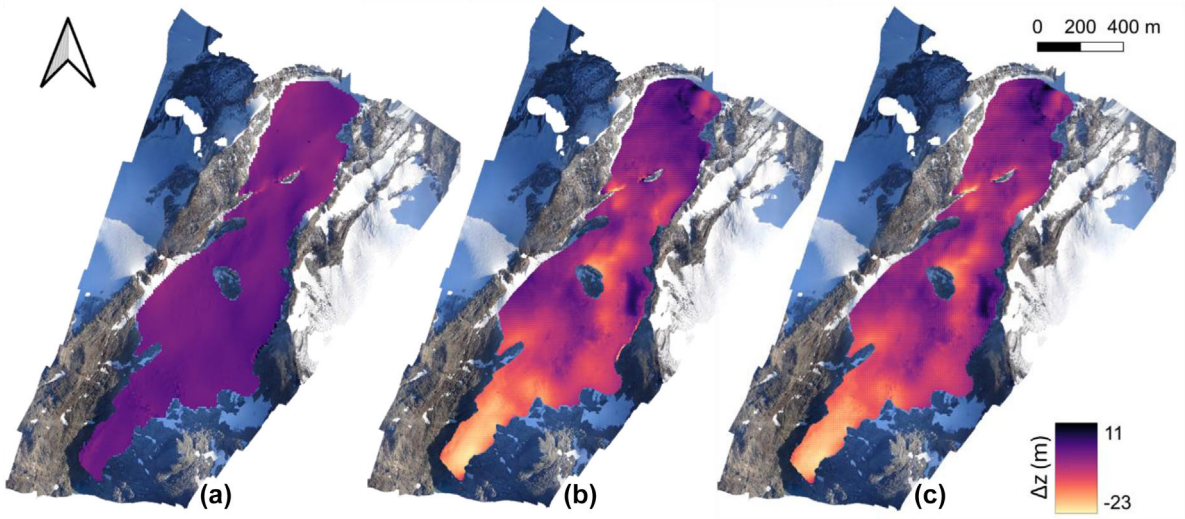

FIGURE 8 Updated ice thickness modelling results: (a) ice thickness estimated with the initial theoretical model only; (b) interpolated GPR ice thickness constraints; (c) ice thickness estimated through the GlaTE algorithm; (d) comparison between the GlaTE and theoretical model.

FIGURE 9 Elevation and ice thickness variations between (a) DTM-1999 and DTM-2008 (2008–1999); (b) DTM-2008 and DEM-2018 (2018–2008); (c) DTM-1999 and DEM-2018 (2018–1999). All the variations are computed inside the glacier perimeter of 2018.

considered reliable. In addition, the error on the slope estimation is generally one order of magnitude lower than the estimated slope.

4 | DISCUSSION

Our analysis integrated data from GPR surveys and glaciological modelling to characterize the ice thickness of the Indren Glacier. Additionally, we examined the impact of recent climatic trends on this glacier dynamics through a comparison of DTMs and temperature records.

4.1 | Ice thickness from GPR data and modelling

Profile 12, presented in Figure 6c, helps to clarify the scattering phenomena encountered in the different radargrams. This profile can indeed be subdivided into a first part, where ice seems transparent to the penetration of the EM waves and the bedrock is clearly identified, and a second part, with a high scattering zone. The shallow features visible in the radargram further help to explain the origin of the scattering. The first part of the line is covered by a thicker and continuous snow cover and clear additional layering can be seen at the interface with

TABLE 2 Estimation of the air temperature trend in the area of the Indren glacier from the daily average temperature records of the closest regional meteorological stations. T_{M1}: trend estimated on the residual temperatures after the removal of the average daily temperatures for each day of the year computed on the whole dataset. T_{M2}: trend estimated on the residual temperatures after the removal of the periodic component of Equation 1.

Station ID	Data period	T_{M1} (°C/year)	T_{M2} (°C/year)
BP	**1988–2023**	**0.038 ± 0.003**	**0.038 ± 0.003**
BP	*until 2005*	*0.025 ± 0.010*	*0.026 ± 0.010*
BP	*since 2005*	*0.070 ± 0.018*	*0.070 ± 0.009*
CM	**2002–2023**	**0.052 ± 0.008**	**0.052 ± 0.008**
GA	**2002–2023**	**0.051 ± 0.007**	**0.051 ± 0.007**

compact ice. In the second part of the radargram, the snowpack is thin and several shallow diffraction hyperbolas are widespread in the section, likely linked to the presence of crevasses, contributing to the infiltration of melting water and modifying the thermal conditions at depth. These diffraction hyperbolas are locally also found at depth, potentially indicating the additional presence of cavities and other melting water paths inside the ice body. The scattering and attenuation of the GPR signal is therefore likely linked to the presence of warm and water-rich ice, as already reported in several studies (e.g., Colombero et al., 2019; Forte et al., 2021). To confirm this, it should be recalled that GPR surveys conducted on the Indren Glacier were performed during the summer period when the high temperatures contribute to snow and ice melting. The existence of warm ice, causing the scattering events, can be therefore directly linked to the presence of crevasses on the glacier surface, through which water percolates, reaching the ice-bedrock interface.

The images generated using the GlaTE model (Figure 8) are quite consistent with the interpolated GPR data (Figure 7). The results of the theoretical glaciological model without the GPR constraints (Figure 8a) already show average thickness values more consistent with the present experimental GPR measurements with respect to the previous models referred to years 1991 (Viani et al., 2020) and 2008 (Figure 1d). This is likely due to the updated geometry and elevation inputs, together with the long temporal gap existent between the different estimates. This consideration stresses on the importance of using input data belonging to coherent time windows to obtain a first rough estimation of the glacier thickness. In the initial model, a deeper ice thickness is also predicted close to the area of the glacier where the over-deepening was found from GPR data interpretation and previous models. However, this over-deepening is shifted 50 m downwards and less extended and pronounced compared to the GPR observations (Figure 8b). Figure 8, in fact, shows a mismatch of 30 m between the theoretical and constrained thickness models in this area. These differences highlight the value of integrating GPR data to refine and improve the accuracy of the final model (Figure 8c).

4.2 | DTM/DEM and temperature analysis

Comparing Figure 9 with the variations in glacier perimeter already highlighted in Figure 1–3, it can be noted that in only 20 years the elevations have dramatically changed, with the biggest variations occurred in the last decade, between 2008 and 2018. Figure 9 well highlights how the thickness reductions have occurred mainly in the frontal area of the glacier, and in the centre, where the rock outcrops have emerged. No significant changes are shown for the period between 1999 and 2008 (Figure 9a), where elevation fluctuations vary within ±2 m, likely linked to the poor resolution of the first DTMs. This is also confirmed by the fact that the variations between 2008 and 2018 (Figure 9b) are highly comparable with those occurred in the whole considered period (Figure 9c).

The thickness modifications depicted over the last two decades are highly in line with the air temperature evolution estimated over the same period. The closest meteorological station (CM), located at higher elevations with respect to the glacier summit, pointed out an extreme temperature trend of approximately 0.05 ± 0.01°C/year in the period from 2002 to the present. Despite the great difference in elevation, this temperature trend is confirmed by the GA station results, active over the same monitoring period. The only station offering more than 30 years of almost continuous daily temperature record (BP) still shows an extreme temperature trend of 0.04°C/year on average, in line with the other two more recent stations.

To compare the temperature trends with the ice thickness evolution during the two decades under investigation (1999–2008 and 2008–2018), we applied the same procedure to the data of the station BP cut in two different datasets of 17 complete years (1989–2005 and 2005–2023). The obtained temperature trends are significantly different: the temperature trend of the second period of observation is more than twice the temperature increase detected until 2005 and closer to the general trend detected by the other two stations. Such high recent temperature rates support the observed higher ice thickness variations in the period between 2008 and 2018 through the DEM analyses. The temperature increase registered in the second decade has led to enhanced ice melting on the Indren Glacier. Thickness variations are an initial manifestation of annual weather conditions (Zemp & Haeberli, 2007). These variations also influence the horizontal length of the glacier over the long term, which is a delayed response to weather conditions and reflects the impact of climate change.

5 | CONCLUSIONS

A two-decade integrated data comparison on the Indren glacier offered a good opportunity to quantify the present ice thickness and investigate thickness variations occurred over a significant time interval. On-site geophysical measurements and remote sensing surveys allowed for the retrieval of an updated ice thickness model for the glacier, while the combination of historical data and long-term temperature records offered consistent information about the thickness evolution over time. Our findings highlight a significant ice thickness decrease in the last decade in comparison to previous time periods and experimentally confirmed the presence of an over-deepening in the glacier, consistent with previous studies. The study relied on basic model inputs and tight data availability, trying to combine discontinuous and freely available spatial data with experimental measurements as a calibration and validation tool. The outcomes underscore the fast response of alpine glaciers to climate change and provide crucial insights for forecasting future scenarios. This simple

integrated approach can be applied to other glacial bodies, contributing to a broader understanding of cryosphere-climate interactions and guiding the research efforts in climate change adaptation and mitigation strategies.

AUTHOR CONTRIBUTION

V.S., C.C. and A.G. designed this research. C.C., F.T. and A.G. acquired the data. V.S., C.C., F.T. and L.M. carried out the data analysis and interpretation. V.S. wrote the first version of the manuscript. All the authors contributed to the review of the first draft and agreed on the final version.

ACKNOWLEDGEMENTS

This publication is part of the project PNRR-NGEU which has received funding from the MUR – DM 118/2023. The authors are also indebted to Diego Franco for the support in GPR data acquisition and Andrea Vergnano for the fruitful discussion on ice thickness modelling. We acknowledge the authors of the public-domain MATLAB TopoToolbox. Open access publishing facilitated by Politecnico di Torino, as part of the Wiley - CRUI-CARE agreement.

DATA AVAILABILITY STATEMENT

The remote sensing and historical data on the Indren Glacier are freely available at https://mappe.partout.it/pub/GeoNavSCT/?repertorio=arpa, https://mappe.regione.vda.it/pub/geonavitg/ and http://catastoghiacciai.partout.it/. The meteorological data are accessible at https://presidi2.regione.vda.it/str_dataview_download and https://www.arpa.piemonte.it/rischi_naturali/snippets_arpa_graphs/map_meteoweb/?rete=stazione_meteorologica. GPR data are available upon request contacting the corresponding author.

ORCID

Valeria Strallo https://orcid.org/0009-0001-9746-2054

REFERENCES

Annan, A.P. (2003) *Ground penetrating radar principles, procedures and applications*. Sensors & Software, Inc, Mississauga, Ontario, Canada.

Beniston, M., Farinotti, D., Stoffel, M., Andreassen, L.M., Coppola, E., Eckert, N., et al. (2018) The European mountain cryosphere: a review of its current state, trends, and future challenges. *The Cryosphere*, 12(2), 759–794. Available from: https://doi.org/10.5194/tc-12-759-2018

Beniston, M. & Stoffel, M. (2014) Assessing the impacts of climatic change on mountain water resources. *Science of the Total Environment*, 493, 1129–1137. Available from: https://doi.org/10.1016/j.scitotenv.2013.11.122

Binder, D., Brückl, E., Roch, K.H., Behm, M., Schöner, W. & Hynek, B. (2009) Determination of total ice volume and ice-thickness distribution of two glaciers in the Hohe Tauern region, Eastern Alps, from GPR data. *Annals of Glaciology*, 50(51), 71–79. Available from: https://doi.org/10.3189/172756409789097522

Brown, L.E., Hannah, D.M. & Milner, A.M. (2007) Vulnerability of alpine stream biodiversity to shrinking glaciers and snowpacks. *Global Change Biology*, 13(5), 958–966. Available from: https://doi.org/10.1111/j.1365-2486.2007.01341.x

Clarke, G.K.C., Anslow, F.S., Jarosch, A.H., Radić, V., Menounos, B., Bolch, T., et al. (2013) Ice volume and subglacial topography for western Canadian glaciers from mass balance fields, thinning rates, and a bed stress model. *Journal of Climate*, 26(12), 4282–4303. Available from: https://doi.org/10.1175/JCLI-D-12-00513.1

Colombero, C., Comina, C., De Toma, E., Franco, D. & Godio, A. (2019) Ice thickness estimation from geophysical investigations on the terminal lobes of belvedere glacier (NW Italian Alps). *Remote Sensing*, 11(7), 805. Available from: https://doi.org/10.3390/rs11070805

Colombo, N., Bocchiola, D., Martin, M., Confortola, G., Salerno, F., Godone, D., et al. (2019) High export of nitrogen and dissolved organic carbon from an Alpine glacier (Indren Glacier, NW Italian Alps). *Aquatic Sciences*, 81(4), 74. Available from: https://doi.org/10.1007/s00027-019-0670-z

Forte, E., Santin, I., Ponti, S., Colucci, R.R., Gutgesell, P. & Guglielmin, M. (2021) New insights in glaciers characterization by differential diagnosis integrating GPR and remote sensing techniques: a case study for the eastern gran Zebrù glacier (Central Alps). *Remote Sensing of Environment*, 267, 112715. Available from: https://doi.org/10.1016/j.rse.2021.112715

Freppaz, M., Williams, M.W., Gabrieli, J., Gorra, R., Mania, I., Ascher-Jenull, J., et al. (2021) Characterization of organic-rich mineral debris revealed by rapid glacier retreat, Indren Glacier, European Alps. *Journal of Mountain Science*, 18(6), 1521–1536. Available from: https://doi.org/10.1007/s11629-020-6288-8

Gärtner-Roer, I., Naegeli, K., Huss, M., Knecht, T., Machguth, H. & Zemp, M. (2014) A database of worldwide glacier thickness observations. *Global and Planetary Change*, 122, 330–344. Available from: https://doi.org/10.1016/j.gloplacha.2014.09.003

Gobiet, A., Kotlarski, S., Beniston, M., Heinrich, G., Rajczak, J. & Stoffel, M. (2014) 21st century climate change in the European Alps—a review. *Science of the Total Environment*, 493, 1138–1151. Available from: https://doi.org/10.1016/j.scitotenv.2013.07.050

Godio, A., Viani, C., Machguth, H., Huggel, C., Perotti, L., & Giardino, M. (2017, April 1). Possible future lakes resulting from continued glacier shrinkage in the Aosta Valley Region (Western Alps, Italy).

Haeberli, W. (2005) Mountain glaciers in global climate-related observing systems. In: Huber, U.M., Bugmann, H.K.M. & Reasoner, M.A. (Eds.) *Global change and mountain regions: an overview of current knowledge*. Netherlands: Springer, 169–175. Available from: https://doi.org/10.1007/1-4020-3508-X_17

Haeberli, W., Hoelzle, M., Paul, F. & Zemp, M. (2017) Integrated monitoring of mountain glaciers as key indicators of global climate change: the European Alps. *Annals of Glaciology*, 46, 150–160. Available from: https://doi.org/10.3189/172756407782871512

Hanzer, F., Förster, K., Nemec, J. & Strasser, U. (2018) Projected cryospheric and hydrological impacts of 21st century climate change in the Ötztal Alps (Austria) simulated using a physically based approach. *Hydrology and Earth System Sciences*, 22(2), 1593–1614. Available from: https://doi.org/10.5194/hess-22-1593-2018

Harris, C., Arenson, L.U., Christiansen, H.H., Etzelmüller, B., Frauenfelder, R., Gruber, S., et al. (2009) Permafrost and climate in Europe: monitoring and modelling thermal, geomorphological and geotechnical responses. *Earth-Science Reviews*, 92(3–4), 117–171. Available from: https://doi.org/10.1016/j.earscirev.2008.12.002

Hock, R., Rasul, G., Adler, C., Cáceres, B., Gruber, S., Hirabayashi, Y., et al. (2019) High mountain areas. In: Pörtner, H.-O., Roberts, D.C., Masson-Delmotte, V., Zhai, P., Tignor, M., Poloczanska, E., *et al.* (Eds.) *IPCC special report on the ocean and cryosphere in a changing climate*. Cambridge University Press, Cambridge, UK and New York, NY, USA, 131–202.

Horton, P., Schaefli, B., Mezghani, A., Hingray, B. & Musy, A. (2006) Assessment of climate-change impacts on alpine discharge regimes with climate model uncertainty. *Hydrological Processes*, 20(10), 2091–2109. Available from: https://doi.org/10.1002/hyp.6197

Huss, M. & Fischer, M. (2016) Sensitivity of very small glaciers in the Swiss Alps to future climate change. *Frontiers in Earth Science*, 4, 34. Available from: https://doi.org/10.3389/feart.2016.00034

IPCC. (2019) Summary for Policymakers. In: Pörtner, H.-O., Roberts, D.C., Masson-Delmotte, V., Zhai, P., Tignor, M., Poloczanska, E., *et al.* (Eds.) *IPCC special report on the ocean and cryosphere in a changing climate*. Cambridge University Press, Cambridge, UK and New York, NY, USA.

Kääb, A., Reynolds, J.M. & Haeberli, W. (2005) Glacier and permafrost hazards in high mountains. In: Huber, U.M., Bugmann, H.K.M. & Reasoner, M.A. (Eds.) *Global change and mountain regions*, Vol. 23. Netherlands: Springer, 225–234. Available from: https://doi.org/10.1007/1-4020-3508-X_23

Langhammer, L., Grab, M., Bauder, A. & Maurer, H. (2019) Glacier thickness estimations of alpine glaciers using data and modeling constraints. *The Cryosphere*, 13(8), 2189–2202. Available from: https://doi.org/10.5194/tc-13-2189-2019

Lemke, P., Ren, J., Alley, R.B., Allison, I., Carrasco, J., Flato, G., et al. (2007) Observations: changes in snow. *Ice and Frozen Ground*. In: Climate Change 2007: The Physical Science Basis. Contribution of Working Group I to theFourth Assessment Report of the Intergovernmental Panel on Climate Change [Solomon, S., D. Qin, M. Manning, Z. Chen, M. Marquis, K.B. Averyt, M. Tignor and H.L. Miller (eds.)]. Cambridge University Press, Cambridge, UK and New York, NY, USA.

Linsbauer, A., Paul, F. & Haeberli, W. (2012) Modeling glacier thickness distribution and bed topography over entire mountain ranges with GlabTop: application of a fast and robust approach. *Journal of Geophysical Research: Earth Surface*, 117, F03007, Available from: https://doi.org/10.1029/2011JF002313

Maggioni, M., Freppaz, M., Piccini, P., Williams, M.W. & Zanini, E. (2009) Snow cover effects on glacier ice surface temperature. *Arctic, Antarctic, and Alpine Research*, 41(3), 323–329. Available from: https://doi.org/10.1657/1938-4246-41.3.323

Mark, B.G. & Fernández, A. (2017) The significance of mountain glaciers as sentinels of climate and environmental change. *Geography Compass*, 11(6), e12318. Available from: https://doi.org/10.1111/gec3.12318

Milner, A.M., Khamis, K., Battin, T.J., Brittain, J.E., Barrand, N.E., Füreder, L., et al. (2017) Glacier shrinkage driving global changes in downstream systems. *Proceedings of the National Academy of Sciences*, 114(37), 9770–9778. Available from: https://doi.org/10.1073/pnas.1619807114

Ogier, C., van Manen, D.-J., Maurer, H., Räss, L., Hertrich, M., Bauder, A., et al. (2023) Ground penetrating radar in temperate ice: englacial water inclusions as limiting factor for data interpretation. *Journal of Glaciology*, 1–12(278), 1874–1885. Available from: https://doi.org/10.1017/jog.2023.68

Owen, L.A., Thackray, G., Anderson, R.S., Briner, J., Kaufman, D., Roe, G., et al. (2009) Integrated research on mountain glaciers: current status, priorities and future prospects. *Geomorphology*, 103(2), 158–171. Available from: https://doi.org/10.1016/j.geomorph.2008.04.019

Patro, E.R., De Michele, C. & Avanzi, F. (2018) Future perspectives of run-of-the-river hydropower and the impact of glaciers' shrinkage: the case of Italian Alps. *Applied Energy*, 231, 699–713. Available from: https://doi.org/10.1016/j.apenergy.2018.09.063

Pepin, N., Bradley, R.S., Diaz, H.F., Baraer, M., Caceres, E.B., Forsythe, N., et al. (2015) Elevation-dependent warming in mountain regions of the world. *Nature Climate Change*, 5(5), 424–430. Available from: https://doi.org/10.1038/nclimate2563

Rabatel, A., Sanchez, O., Vincent, C. & Six, D. (2018) Estimation of glacier thickness from surface mass balance and ice flow velocities: a case study on Argentière glacier, France. *Frontiers in Earth Science*, 6, 112, Available from: https://doi.org/10.3389/feart.2018.00112

Salim, E., Ravanel, L., Bourdeau, P. & Deline, P. (2021) Glacier tourism and climate change: effects, adaptations, and perspectives in the Alps. *Regional Environmental Change*, 21(4), 120. Available from: https://doi.org/10.1007/s10113-021-01849-0

Santin, I., Roncoroni, G., Forte, E., Gutgesell, P. & Pipan, M. (2024) GPR modelling and inversion to quantify the debris content within ice. *Near Surface Geophysics*, 22(2), 220–234. Available from: https://doi.org/10.1002/nsg.12274

Singh, S.K., Rathore, B.P., Bahuguna, I.M. & Ramnathan, A.L. (2012) Estimation of glacier ice thickness using ground penetrating radar in the Himalayan region. *Current Science*, 103(1), 68–73.

Solomon, S., Qin, D., Manning, M., Chen, Z., Marquis, M., Averyt, K., et al. (2007) IPCC, 2007: climate change 2007: the physical science basis. In: *Contribution of working group I to the fourth assessment report of the intergovernmental panel on climate change*. Cambridge university press, Cambridge, UK and New York, NY, USA.

Tognetto, F., Perotti, L., Viani, C., Colombo, N. & Giardino, M. (2021) Geomorphology and geosystem services of the Indren-Cimalegna area (Monte Rosa massif – Western Italian Alps). *Journal of Maps*, 17(2), 161–172. Available from: https://doi.org/10.1080/17445647.2021.1898484

Van Tricht, L. & Huybrechts, P. (2023) Modelling the historical and future evolution of six ice masses in the Tien Shan, Central Asia, using a 3D ice-flow model. *The Cryosphere*, 17(10), 4463–4485. Available from: https://doi.org/10.5194/tc-17-4463-2023

Viani, C., Machguth, H., Huggel, C., Godio, A., Franco, D., Perotti, L., et al. (2020) Potential future lakes from continued glacier shrinkage in the Aosta Valley region (Western Alps, Italy). *Geomorphology*, 355, 107068. Available from: https://doi.org/10.1016/j.geomorph.2020.107068

Winkler, S., Chinn, T., Gärtner-Roer, I., Nussbaumer, S.U., Zemp, M. & Zumbühl, H.J. (2010) An Introduction to mountain glaciers as climate indicators with spatial and temporal diversity. *Erdkunde*, 64(2), 97–118. Available from: https://doi.org/10.3112/erdkunde.2010.02.01

Zekollari, H., Huss, M. & Farinotti, D. (2019) Modelling the future evolution of glaciers in the European Alps under the EURO-CORDEX RCM ensemble. *The Cryosphere*, 13(4), 1125–1146. Available from: https://doi.org/10.5194/tc-13-1125-2019

Zekollari, H., Huss, M., Farinotti, D. & Lhermitte, S. (2022) Ice-dynamical glacier evolution modeling—a review. *Reviews of Geophysics*, 60(2), e2021RG000754. Available from: https://doi.org/10.1029/2021RG000754

Zemp, M., & Haeberli, W. (2007). Glaciers and ice caps. Part I: global overview and outlook. Part II: glacier changes around the world. Available from: https://doi.org/10.5167/UZH-40427

Zemp, M., Haeberli, W., Hoelzle, M. & Paul, F. (2006) Alpine glaciers to disappear within decades? *Geophysical Research Letters*, 33, L13504, Available from: https://doi.org/10.1029/2006GL026319

SUPPORTING INFORMATION

Additional supporting information can be found online in the Supporting Information section at the end of this article.

How to cite this article: Strallo, V., Colombero, C., Troilo, F., Mondardini, L. & Godio, A. (2025) Glacier thickness modelling and monitoring with geophysical data constraints: A case study on the Indren Glacier (NW Italy). *Earth Surface Processes and Landforms*, 50(1), e6068. Available from: https://doi.org/10.1002/esp.6068